Wideband Metasurface-Based Reflective Polarization Converter for Linear-to-Linear and Linear-to-Circular Polarization Conversion

Qi Zheng, *Student Member, IEEE*, Chenjiang Guo, and Jun Ding

***Abstract*—A wideband reflective polarization converter based on metasurface is proposed in this letter. This converter can transform a linearly polarized (LP) incident electromagnetic (EM) wave into its orthogonal LP reflection wave in a lower band, and a circularly polarized (CP) reflection wave in a higher band. The unit cell of this converter is comprised of two meander lines and one cut wire printed on a dielectric substrate, backed with metallic ground sheet. The simulation results show that the *y*/*x*-polarized incident EM wave can be converted to the *x*/*y*-polarized reflected wave over a fractional bandwidth of 59.6% from 6.53 to 12.07 GHz with a polarization conversion ratio over 0.88. Besides, the *y*/*x*-polarized incident EM wave is converted to a CP reflected wave from 13.70 to 15.60 GHz (a fractional bandwidth of 13.0%). To verify the polarization conversion performance, a sample consisting of 30 × 30 unit cells is fabricated and measured. The experimental and simulation results obtained are in a reasonable agreement, which verifies the properties of the design.**

***Index Terms*—Metasurface, polarization converter, wideband.**

I. Introduction

POLARIZATION converters, for their special properties in polarization manipulation, have been applied a lot in microwave, terahertz, and even optical frequencies [1]–[5]. However, conventional structures for manipulating polarization, such as optical activity crystals, require a much larger thickness, compared to the operating wavelength. To overcome this issue, metamaterials, such as anisotropic metamaterials [6]–[10] and chiral metamaterials [11]–[14], have been widely employed in many studies.

Recently, the reflective polarization converters based on metasurface were proposed [15]–[22]. Metasurface, a planar metamaterial, has been utilized in perfect polarization conversion (PC) with broad bandwidth for its strong anisotropy and multiple plasmon resonances [15]. There are many different metasurface-based polarization coveters, such as double-head arrow [16], oval-ring resonator [17], double V-shaped patches [18], L-shaped patches [19], and double triangular split rings [20], that have been introduced to achieve wideband cross polarization conversion. In [21], an I-shaped structure was presented to convert a linearly polarized (LP) incident wave to a circularly polarized (CP) reflection with a fractional bandwidth of 15%. A cross/ring resonator [22] was given to achieve a linear polarization, converted to a cross polarization or a circular polarization, by adjusting parameters. Double-L-shaped metasurface [23] was also introduced to design multipolarization converter, which can convert an LP incident wave to a CP reflected wave at four bands of 5.5–6.1, 12.1–16, 6.65–9.6, and 18.1–22.5 GHz. Besides, the reflected wave is along the cross-polarized direction at three bands of 6.15–6.45, 10.2–11.45, and 16.25–17.6 GHz. In addition, a double-split square-ring resonator [24] was applied to achieve a linear-to-circular polarization conversion with 80% fractional bandwidth at terahertz frequencies. However, there are few research works on converting a linear polarization to a cross polarization and a circular polarization over wideband simultaneously.

In this letter, we propose a metasurface-based polarization converter to convert an LP incident electromagnetic (EM) wave into an LP reflection wave in a lower band, and a CP reflection wave in a higher band. The letter is organized as follows: Section II presents the design and analysis of the proposed metasurface. Section III gives the measured results of the fabricated sample. Finally, concluding remarks are drawn in Section IV.

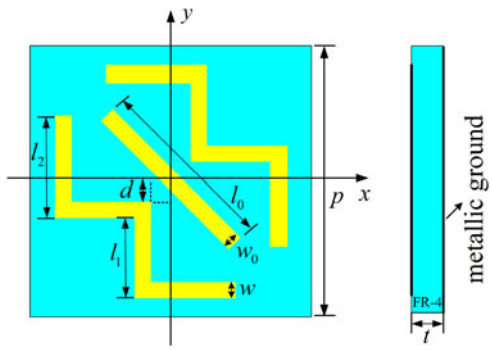

Fig. 1. Schematic of the unit cell.

II. Design and Analysis of the Metasurface

A. Configuration of Unit Cell

Schematic of the unit cell of the proposed polarization converter is shown in Fig. 1. There are three parts: 1) a top metal-

Manuscript received May 4, 2018; revised May 29, 2018 and June 10, 2018; accepted June 17, 2018. Date of publication June 21, 2018; date of current version August 2, 2018. This work was supported by the Excellent Doctorate Cultivating Foundation of Northwestern Polytechnical University. *(Corresponding author: Qi Zheng.)*

The authors are with the School of Electronics and Information, Northwestern Polytechnical University, Xi'an 710072, China (e-mail: zhq930908@mail.nwpu.edu.cn; cjguo@nwpu.edu.cn; dingjun@nwpu.edu.cn).

Digital Object Identifier 10.1109/LAWP.2018.2849352

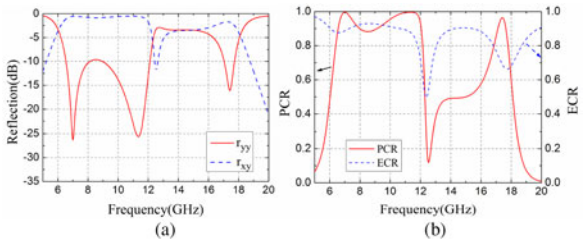

Fig. 2. (a) Co- and cross-polarized reflection coefficients. (b) PCR and ECR versus frequency.

lic copper structure; 2) a middle dielectric substrate; and 3) a bottom metallic ground plate. The top metallic structure is comprised of two symmetric meander lines and one cut-wire structure, which is placed -45° along the $+y$-axis. The middle substrate is the FR-4 with a dielectric constant of 4.4 and a dielectric loss tangent of 0.02. The bottom metallic ground is the copper with a conductivity of 5.8×10^7 S/m and a thickness of 0.035 mm. Here, we adopt EM simulation software Ansoft HFSS ver. 13.0 to obtain a linear-to-linear polarization conversion in the lower band and a linear-to-circular polarization conversion in the higher band. The unit cell is simulated with Floquet port in the $+z$-direction and master/slave boundaries the in x- and y-direction. Final parameters are shown as follows: $p = 8.1$ mm, $t = 3.1$ mm, $d = 0.4$ mm, $l_1 = 2.5$ mm, $w = 0.3$ mm, $l_2 = 2.3$ mm, $l_0 = 6$ mm, $w_0 = 0.3$ mm.

Taking a y-polarized incident wave as an example, we define $r_{xy} = |\vec{E}_x^r / \vec{E}_y^i|$ and $r_{yy} = |\vec{E}_y^r|/|\vec{E}_y^i|$ to represent PC properties of the cross polarization (y-to-x) and the copolarization (y-to-y), respectively. Polarization conversion ratio (PCR) is defined as $\text{PCR} = r_{xy}^2/(r_{xy}^2 + r_{yy}^2)$ to evaluate its PC characteristics. The co- and cross polarizations are shown in Fig. 2(a). We can see that the copolarization is below -9.6 dB from 6.53 to 12.07 GHz and the co- and cross polarizations are almost equal from 13.90 to 15.30 GHz. From Fig. 2(b), it is found that the PCR is over 0.88 from 6.53 to 12.07 GHz. This indicates that the LP incident wave is rotated to its orthogonal LP reflection wave with high-PC efficiency. Two resonance frequencies occur at 7.00 and 11.34 GHz. The PCR is 0.5 ± 0.01 from 13.90 to 15.30 GHz, and 0.5 PCR occurs at 15.00 GHz. This means about half of the energy is converted into its orthogonal direction. The energy conversion ratio (ECR) [24] is employed to indicate total energy conversion efficiency, and is defined as $\text{ECR} = (|\vec{E}_x^r|^2 + |\vec{E}_y^r|^2)/|\vec{E}_y^i|^2 = r_{xy}^2 + r_{yy}^2$.

It also can be seen from Fig. 2(b) that the efficiency of the CP is over 0.89 (from 13.70 to 15.60 GHz). These results show that the proposed structure exhibits high-efficiency conversion property.

In the next step, we employ azimuth angle ($\eta = \arctan(|\vec{E}_x^r|/|\vec{E}_y^r|), [0^\circ, 90^\circ]$) and axial ratio (AR) (dB,

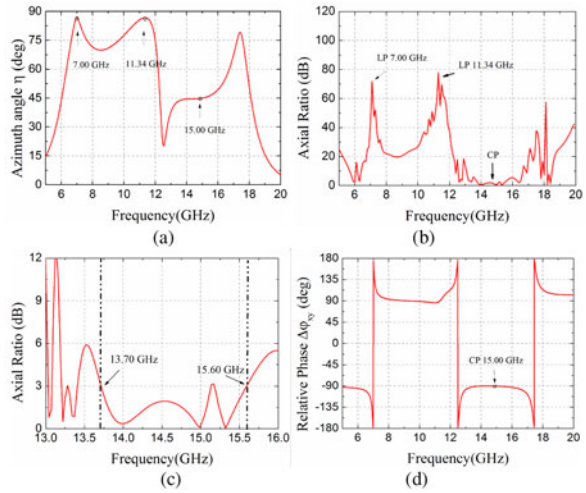

Fig. 3. (a) η. (b) AR versus frequency. (c) Detailed CP bandwidth. (d) Detailed phase difference.

$0 \le \text{AR} \le \infty$) of the reflection to evaluate polarization states of reflected EM wave, where phase difference between the total reflected field along the x- and y-axis ($\Delta\varphi_{xy} = \varphi_x - \varphi_y, [-180^\circ, 180^\circ]$) is given to study detailed circular polarization states, as shown in Fig. 3. It is noted that the reflection is an ideal linear polarization ($AR = \infty$), when $\eta = 90^\circ$ and a perfect circular polarization ($AR = 0$) is generated when $\eta = 45^\circ$ and $\Delta\varphi_{xy} = \pm 45^\circ$. The others are ellipse polarizations. In this letter, we adopt a 3 dB AR bandwidth to evaluate its circular-polarization property.

The value of the AR can be calculated by (1) shown at the bottam of this page, where the angle of the polarized ellipse as τ

$$\tan(2\tau) = \frac{2\left(\left|\vec{E}_x^r\right|\exp(-j\varphi_x)\right)\left(\left|\vec{E}_y^r\right|\exp(-j\varphi_y)\right)}{\left(\left|\vec{E}_x^r\right|\exp(-j\varphi_x)\right)^2 - \left(\left|\vec{E}_y^r\right|\exp(-j\varphi_y)\right)^2}\cos(\Delta\varphi_{xy}). \tag{2}$$

The normalized format is given by

$$AR = |r_{AR}|_{dB} = 20\log_{10}(r_{AR}). \tag{3}$$

As presented in Fig. 3(a), the azimuth angles are 87.05° and 86.79° at 7.00 and 11.34 GHz, which indicate that the reflected waves are linear polarizations. At 15.00 GHz, the azimuth angle equals 45°, which means that the magnitudes between x- and y-components of the reflected field are equal. It also indicates the potential candidate for a circular polarization. As can be seen from Fig. 3(b), the values of AR are over 70 dB at two resonance frequencies (7.00 and 11.34 GHz), which indicate that the reflection waves are linear polarizations. The detailed curves are given in Fig. 3(c). It can be seen that the 3 dB AR

$$r_{AR} = \frac{\left(\left|\vec{E}_x^r\right| / \left|\vec{E}_y^r\right|\right)\cos^2(\tau) + \sin(2\tau)\cos(\Delta\varphi_{xy}) + \left(\left|\vec{E}_x^r\right| / \left|\vec{E}_y^r\right|\right)\sin^2(\tau)}{\left(\left|\vec{E}_x^r\right| / \left|\vec{E}_y^r\right|\right)\sin^2(\tau) - \sin(2\tau)\cos(\Delta\varphi_{xy}) + \left(\left|\vec{E}_x^r\right| / \left|\vec{E}_y^r\right|\right)\cos^2(\tau)} \tag{1}$$

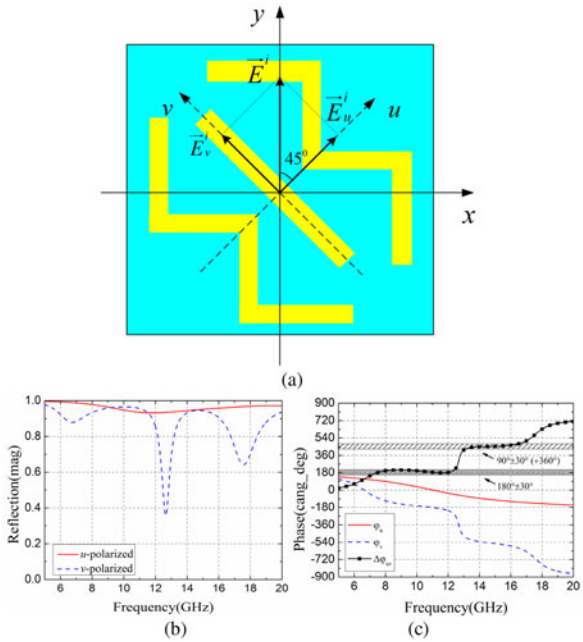

Fig. 4. (a) New coordinate system *uv*-axis. (b) Refection magnitudes and (c) reflection phases under *u*- and *v*-polarization and the phase difference.

bandwidth is obtained from 13.70 to 15.60 GHz. The phase difference given in Fig. 3(d) satisfies $\Delta\varphi_{xy} = -90°$. Therefore, the reflection wave is a right-hand circular polarization.

B. Analysis of Polarization Conversion

The unit cell of polarization converter is designed on the basis of antistrophic structure, which is evolved from a cut-wire resonator [5]. Thus, we define anisotropic coordinate system (*uv*-axis) to study its mechanisms of PC. The *u*- and *v*-axes are $\pm 45°$ along the $+y$-direction, respectively, as shown in Fig. 4(a). Taking an LP incident wave along $+y$-axis illuminate on the structure as an example, the incident EM wave can be decomposed into two equal components ($\vec{E}_u^i$ and $\vec{E}_v^i$). It can be expressed as

$$\vec{E}_y^i = \frac{\sqrt{2}}{2}\left|\vec{E}_y^i\right|\exp(jkz)\,\vec{e}_u + \frac{\sqrt{2}}{2}\left|\vec{E}_y^i\right|\exp(jkz)\,\vec{e}_v. \quad (4)$$

The reflected wave can be expressed as

$$\vec{E}_{\text{total}}^r = \frac{\sqrt{2}}{2}|\Gamma_u|\left|\vec{E}_y^i\right|\exp(-jkz+\varphi_u)\,\vec{e}_u + \frac{\sqrt{2}}{2}|\Gamma_v|\left|\vec{E}_y^i\right|\exp(-jkz+\varphi_v)\,\vec{e}_v \quad (5)$$

The energy of incident wave can be treated as totally reflected, without considering that dielectric losses for the structure are backed with a metallic sheet ($|\Gamma_u| \cong |\Gamma_v|$). Therefore, the conditions of the LP and the CP can be determined by

$$\Delta\varphi_{uv} = |\varphi_u - \varphi_v| = 2n\pi + \pi \quad (n = 0, 1, 2\ldots)\,\text{LP} \quad (6a)$$

$$\Delta\varphi_{uv} = |\varphi_u - \varphi_v| = 2n\pi \pm \pi/2 \quad (n = 0, 1, 2\ldots)\,\text{CP} \quad (6b)$$

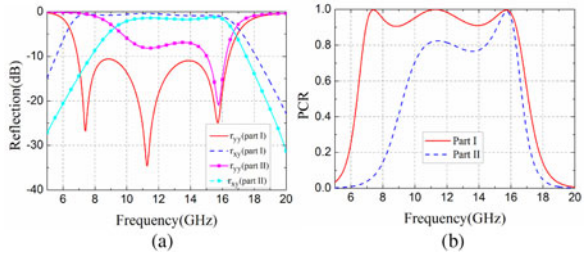

Fig. 5. (a) Co- and cross-polarized reflection coefficients. (b) PCR versus frequency.

The reflection magnitudes, reflection phases under the *u*- and *v*-polarized directions (namely φ_u and φ_v), and phase difference ($\Delta\varphi_{uv} = |\varphi_u - \varphi_v|$) between the *u*- and the *v*-axes are given in Fig. 4(b) and (c). It can be found that the differences between the reflected magnitudes along *uv*-axis are less than 0.1 in the bands of 7.06–11.75 and 12.85–16.43 GHz. The reflection phase differences are roughly 180° from 7.17 to 12.40 GHz and around 90° from 13.05 to 16.52 GHz, respectively. These indicate that the proposed structure has the potential to convert the LP EM wave into LP and CP reflection waves in a lower band and higher band, respectively.

The design procedure mainly contains three steps: 1) design of two symmetric meander lines (namely part I); 2) design of one cut-wire resonator (namely part II); and 3) optimization of the parameters. The main purpose of the first step is to obtain a wideband high PCR, which ensures that the LP incident wave can be rotated to its orthogonal LP reflection. The function of the cut-wire resonator, which is about 0.6 times the physical length of the meander-line resonator, proposed at step 1, is to disturb polarization states and achieve a circular polarization in the higher band. Finally, the structure is optimized to realize an LP reflection wave in the lower band as well as a CP reflection wave in the higher band.

The co- and cross-polarized reflection coefficients and the PCR of parts I and II are illustrated in Fig. 5. It can be seen that the part I generates lower than -10 dB copolarization (r_{yy}) from 6.92 to 16.42 GHz and over 0.9 PCR from 6.95 to 16.33 GHz. The frequency discrepancy between the copolarization and the PCR bandwidth is mainly caused by the dielectric losses. Three resonance frequencies occur at 7.39, 11.25, and 15.71 GHz with nearly 100% PC. As for part II, it can be found that it has less contribution on PC in the lower band, but has much more contribution on the higher band. It achieves over 0.8 PCR from 10.69 to16.15 GHz, and one peak value occurs at 15.76 GHz with nearly 100% polarization conversion.

In addition, the azimuth angle and the phase difference between the total reflected fields along the *x*- and *y*-axes and the AR of the reflection wave are given in Fig. 6. As presented in Fig. 6(a), the azimuth angle of part I and the proposed structure have a good consistency in the lower band (5–12 GHz). These validate that the part II has little impact in low frequency. However, the curve of the proposed structure descends rapidly and then keeps steady with $\eta = 45°$ in the higher band, with respect to part I. It is expected for the influence of part II, which mainly operates in the higher band. Fig. 6(b) depicts AR values

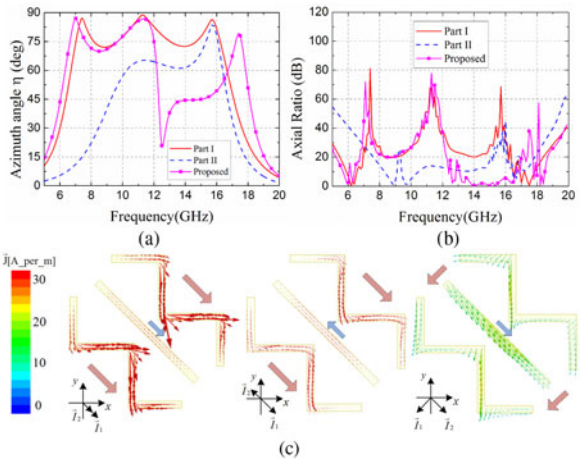

Fig. 6. (a) Azimuth angle η. (b) AR versus frequency. (c) Induced surface current distributions at 7.00, 11.34, and 15.00 GHz.

versus frequency of parts I, II, and the proposed structure. It is obvious that the polarization state of the reflected EM wave converted by parts I and II is either a linear polarization or an elliptic polarization, while the reflected EM wave converted by the proposed structure is a linear polarization in the lower band and a circular polarization in the higher band.

Moreover, inspired by the explanation introduced by Li *et al.* [10], the induced surface current distributions at three resonance frequencies (7.00, 11.34, and 15.00 GHz) are displayed in Fig. 6(c). The currents are fixed on part I in the lower band and part II in the higher band. This phenomenon also validates the different functions of parts I and II. At 7.00 GHz, both the equivalent currents of parts I ($\vec{I}_1$) and II ($\vec{I}_2$) flow along the same diagonal direction. At 11.34 GHz, the equivalent currents of parts I ($\vec{I}_1$) and II ($\vec{I}_2$) flow along two opposite diagonal directions, respectively. These results indicate that the reflected wave is a linear polarization. At 15.00 GHz, the equivalent currents of parts I ($\vec{I}_1$) and II ($\vec{I}_2$) flow along two orthogonal diagonal directions, which results in a CP reflection wave.

III. Measurement

To verify the simulations, a sample consisting of 30 × 30 unit cells with a total dimension of 243 mm × 243 mm × 3.1 mm was fabricated and measured. The sample and schematic views of measurement are shown in Fig. 7(a) and (b), respectively. Due to the difficulties associated with the reflection-phase measurement, only reflection coefficients were measured in a microwave anechoic chamber. Two standard LP horn antennas connected with a network analyzer are placed along the same direction operating for transmitting and receiving signals, respectively. The measured results are normalized with equal-sized metallic plate. The measured and simulated results are shown in Fig. 7(c). It can be concluded that the measurement and simulation results are in a reasonable agreement. The discrepancies are acceptable, considering fabrication and measurement errors, such as misalignment of the horn antennas and noises in the background.

Comparisons with other reported wideband single-layer metasurface-based reflective polarization converters are

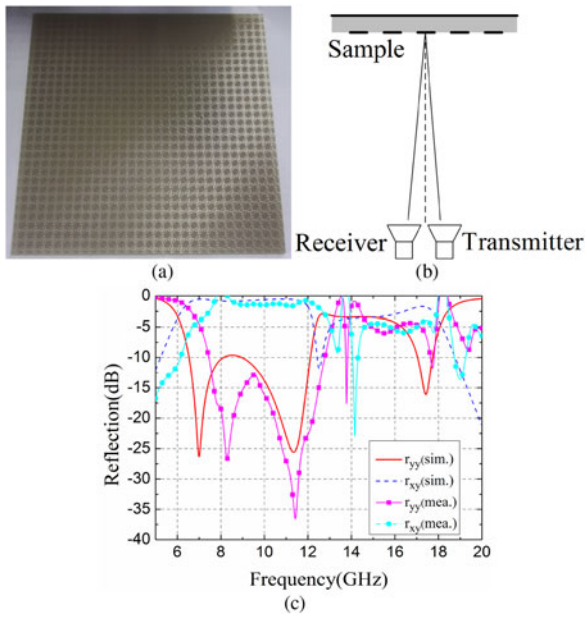

Fig. 7. (a) Front view of the fabricated sample. (b) Schematic view of the measurement setup. (c) Measured and simulated reflection coefficients.

TABLE I
Performance Comparisons of Polarization Converters. CF: Center Frequency. PCP: Polarization Conversion Property. FBW: Fractional Bandwidth of PCR > 0.88 (Linear-to-Linear) or AR < 3 dB (Linear-to-Circular)

Works	CF(GHz)	PCP	FBW (%)
Re[18]	20.18	Linear-to-Linear	77
Re[22]	13.55	Linear-to-Circular	30.3
this paper	9.30 14.65	Linear-to-Linear Linear-to-Circular	59.6 13.0

included in Table I. It can be observed that the proposed design has a comparable wideband in achieving a linear-to-linear and a linear-to-circular polarization conversion simultaneously.

IV. Conclusion

In this letter, a wideband and high-efficiency reflective polarization converter based on metasurface is proposed to convert the LP incident EM into its orthogonal LP reflection wave in a lower band and a CP reflection wave in a higher band. The simulation results demonstrate that it achieves greater than 0.88 PCR from 6.53 to 12.07 GHz for a linear-to-linear polarization conversion. Besides, a fractional bandwidth of 13. 0% from 13.70 to 15.60 GHz for a linear-to-circular polarization conversion can also be obtained. The experimental results are in a reasonable agreement with the simulations. The proposed design may have potential applications in polarization-manipulation devices and antenna design for its linear-to-linear and linear-to-circular polarization conversion properties.

REFERENCES

[1] H. L. Zhu, S. W. Cheung, K. L. Chung, and T. I. Yuk, "Linear-to-circular polarization conversion using metasurface," *IEEE. Trans. Antennas Propag.*, vol. 61, no. 9, pp. 4615–4623, Sep. 2013.

[2] W. Yang, K.-W Tam, W. W. Choi, W. Che, and H. T. Hui, "Polarisation rotation reflective surface based on artificial magnetic conductor and its application," *Electron. Lett.*, vol. 50, no. 21, pp. 1500–1502, 2014.

[3] Q. Zheng, C. Guo, Y. Qu, and J. Ding, "Design of broadband circularly polarized reflectarray with linearly polarized feed," in *Proc. Asia-Pac. Microw. Conf.*, New Delhi, India, 2016, pp. 1–3.

[4] L. Cong *et al.*, "Manipulating polarization states of terahertz radiation using metamaterials," *New J. Phys.*, vol. 14, no. 11, Nov. 2012, Art. no. 115013.

[5] N. K. Grady *et al.*, "Terahertz metamaterials for linear polarization conversion and anomalous refraction," *Science*, vol. 340, no. 6138, pp. 1304–1307, Jun. 2013.

[6] J. Hao *et al.*, "Manipulating electromagnetic wave polarizations by anisotropic metamaterials," *Phys. Rev. Lett.*, vol. 99, Aug. 2007, Art. no. 063908.

[7] J. Y. Chin, M. Lu, and T. J. Cui, "Metamaterials polarizers by electric-field-coupled resonators," *Appl. Phys. Lett.*, vol. 93, 2008, Art. no. 251903.

[8] R. Singh *et al.*, "Terahertz metamaterial with asymmetric transmission," *Phys. Rev. B*, vol. 80, Oct. 2009, Art. no. 153104.

[9] C. Menzel *et al.*, "Asymmetric transmission of linearly polarized light at optical metamaterials," *Phys. Rev. Lett.*, vol. 104, Jun. 2010, Art. no. 253902.

[10] Y. Li *et al.*, "Achieving wide-band linear-to-circular polarization conversion using ultra-thin bi-layered metasurfaces," *J. Appl. Phys.*, vol. 117, no. 4, 2015, Art. no. 044501.

[11] Y. Ye and S. He, "90° polarization rotator using a bilayered chiral metamaterial with giant optical Activity," *Appl. Phys. Lett.*, vol. 96, 2010, Art. no. 203501.

[12] J. H. Shi *et al.*, "Dual-band asymmetric transmission of linear polarization in bilayered chiral metamaterial," *Appl. Phys. Lett.*, vol. 102, 2013, Art. no. 191905.

[13] C. Pfeiffer and A. Grbic, "Bianisotropic metasurfaces for optimal polarization control: analysis and synthesis," *Phys. Rev. Appl.*, vol. 2, Oct. 2014, Art. no. 044011.

[14] S. Yan and G. A. Vandenbosch, "Compact circular polarizer based on chiral twisted double split-ring resonator," *Appl. Phys. Lett.*, vol. 102, 2013, Art no. 103503.

[15] M. Feng *et al.*, "Broadband polarization rotator based on multi-order plasmon resonances and high impedance surfaces," *J. Appl. Phys.*, vol. 114, 2013, Art. no. 074508.

[16] H. Chen *et al.*, "Ultra-wideband polarization conversion metasurfaces based on multiple plasmon resonances," *J. Appl. Phys.*, vol. 115, 2014, Art. no. 154504.

[17] L. Zhang, P. Zhou, H. Lu, H. Chen, J. Xie, and L. Deng, "Ultra-thin reflective metamaterial polarization rotator based on multiple plasmon resonances" *IEEE Antennas Wireless Propag. Lett.*, vol. 14, pp. 1157–1160, 2015.

[18] X. Gao, X. Han, W.-P Cao, H. O. Li, H. F. Ma, and T. J. Cui, "Ultrawideband and high-efficiency linear polarization converter based on double V-shaped metasurface," *IEEE Trans Antennas Propag*., vol. 63, no. 8, pp. 3522–3530, Aug. 2015.

[19] Y. Jia, Y. Liu, W. Zhang, and S. Gong, "Ultra-wideband and high-efficiency polarization rotator based on metasurface," *Appl. Phys. Lett.*, vol. 109, 2016, Art. no. 051901.

[20] Q. Zheng, C. Guo, H. Li, and J. Ding, "Wideband and high-efficiency reflective polarization rotator based on metasurface," *J. Electromagn. Wave*, vol. 32, no. 3, pp. 265–273, 2018.

[21] H. F. Ma, G. Z. Wang, G. S. Kong, and T. J. Cui, "Broadband circular and linear polarization conversions realized by thin birefringent reflective metasurfaces," *Opt. Mater. Express*, vol. 4, no. 8, pp. 1717–1724, 2014.

[22] Z. Zhang, X. Cao, J. Gao, and L. Sijia, "Broadband metamaterial reflectors for polarization manipulation based on cross/ring resonators," *Radioengineering*, vol. 25, no. 3, pp. 436–441, 2016.

[23] C. Mao, Y. Yang, X. He, J. Zheng, and C. Zhou, "Broadband reflective multi-polarization converter based on single-layer double-L-shaped metasurface," *Appl. Phys. A.*, vol. 123, Dec. 2017, Art. no. 767.

[24] Y. Jiang, L. Wang, J. Wang, C. N. Akwuruoha, and W. Cao, "Ultra-wideband high-efficiency reflective linear-to-circular polarization converter based on metasurface at terahertz frequencies," *Opt. Express*, vol. 25, no. 22, pp. 27616–27623, 2017.